




When does entropy promote local organization?†

Cite this: DOI: 10.1039/c9sm02540e

 Andrei A. Klishin ^{abc} and Greg van Anders ^{*abd}

 Received 29th December 2019,
 Accepted 8th June 2020

DOI: 10.1039/c9sm02540e

rsc.li/soft-matter-journal

Crowded soft-matter and biological systems organize locally into preferred motifs. Locally-organized motifs in soft systems can, paradoxically, arise from a drive to maximize overall system entropy. Entropy-driven local order has been directly confirmed in model, synthetic colloidal systems, however similar patterns of organization occur in crowded biological systems ranging from the contents of a cell to collections of cells. In biological settings, and in soft matter more broadly, it is unclear whether entropy generically promotes or inhibits local organization. Resolving this is difficult because entropic effects are intrinsically collective, complicating efforts to isolate them. Here, we employ minimal models that artificially restrict system entropy to show that entropy drives systems toward local organization, even when the model system entropy is below reasonable physical bounds. By establishing this bound, our results suggest that entropy generically promotes local organization in crowded soft and biological systems of rigid objects.

1 Introduction

The mechanisms that drive behaviours in crowded molecular, soft-material, and biological environments can be difficult to infer. Difficulties arise not only because there are many competing interaction types,^{1,2} but also because of the frequent and ambiguous role played by entropy.^{2–10} Entropic effects are inherently collective and emergent in nature, complicating attempts to detect them. The detection of entropic effects in soft matter has been aided, in colloids, by the identification and measurement of directional entropic forces (DEFs).⁶ DEFs drive crowded particles or bodies to undergo local organization. Organization that occurs in order to maximize entropy is a counterintuitive phenomenon, but it has been directly observed, *via* DEFs, in several colloidal systems.^{11–17} Similar effects of entropy-driven local organization have been observed in pseudothermally-driven granular systems¹⁸ and in biological contexts, *e.g.* in virus–membrane interactions,⁸ in diseases that affect red blood cell rheology,^{3,9,19} and in models of crowded membranes.²⁰ The multiplicity of settings in which entropy is implicated in the local organization of crowded entities raises the question: are known settings isolated instances, each associated with specific system features? Or, are known instances

examples of a widespread phenomenon? The answer depends on understanding: when does entropy promote local organization?

Longstanding,²¹ general intuition that entropy is synonymous with disorder would suggest that entropic effects should generically act to inhibit rather than promote organization. In other words, intuition suggests that the entropic promotion of local order should be rare. However, similar intuition that entropy should favour global disorder,²² meant that the existence of entropy-driven global order was known for some time^{23–26} before it was understood to be a widespread phenomenon in hard colloids^{6,27–32} that was not simply a matter of global dense packing.³³ The possibility that the entropic promotion of local order is more widespread could be obviously masked or limited by other competing interactions (see, *e.g.*, ref. 34). For local organization, as in the global order case, a more subtle and fundamental question is: when is the phenomenon of entropy-driven local organization masked or limited by the counterintuitive and collective nature of entropy itself?

To understand the potential range of systems that can manifest an entropic preference for local organization, it is important to look for limitations on the phenomenon suggested by prior work. Prior works have shown that a variety of selected, crowded systems that possess a continuum “sea” of microstates have objects that are driven to adopt preferred local arrangements.⁶ The fact that entropy-driven local organization has been, thus far, observed in the presence of continuum sea entropy suggests that a potential route to eliminate or bound the effect is simply to construct an appropriate model system that eliminates a large part of the entropy that drives local organization.

Here, we attempt to bound the ubiquity of entropy-driven local organization by artificially “subtracting” a substantial portion of the entropy that leads to the emergence of local order in other

^a Department of Physics, University of Michigan, Ann Arbor, MI 48109, USA

^b Center for the Study of Complex Systems, University of Michigan, Ann Arbor, MI 48109, USA

^c John A. Paulson School of Engineering and Applied Sciences, Harvard University, Cambridge, MA 02138, USA

^d Department of Physics, Engineering Physics, and Astronomy, Queen's University, Kingston, ON K7L 3N6, Canada. E-mail: gva@queensu.ca

† Electronic supplementary information (ESI) available. See DOI: 10.1039/c9sm02540e

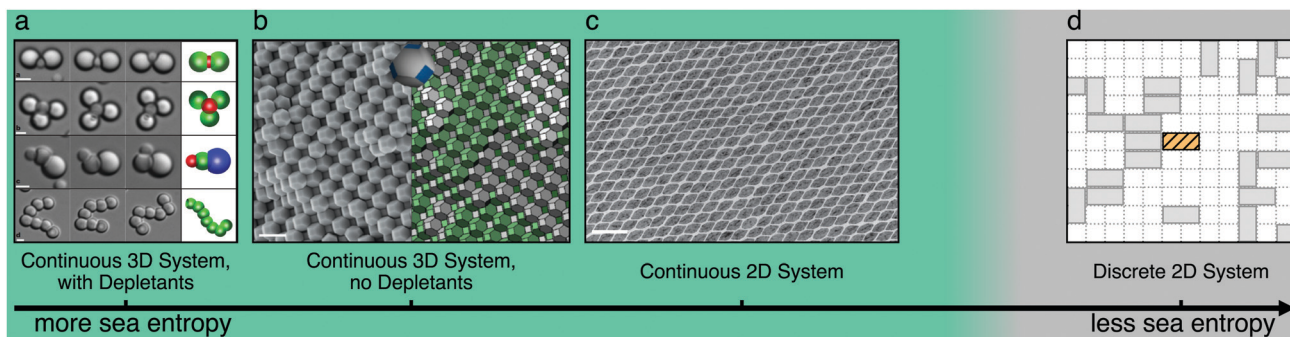


Fig. 1 Examples of entropy-driven organization can be ordered by the amount of “sea particle” entropy, decreasing from left to right. Entropic ordering in systems (a–c) has been demonstrated in prior works (green background shade), but it is unclear whether it persists all the way down to system (d) (gray background shade). (a) Self-assembly of depletant-driven 3D lock-and-key junctions from silica spheres and dimpled spheres. Imaged by optical microscopy, scale bar is 2 μm . Adapted from ref. 35. (b) Self-assembly of the 3D space filling Kelvin structure, corresponding to the body centred cubic lattice, from truncated octahedral Ag nanocrystals. (left) Scanning electron microscopy micrograph, scale bar is 500 nm; (right) computer-generated densest lattice. Adapted from ref. 36. (c) Self-assembly of 2D superlattices from lanthanide fluoride nanoplatelets. Imaged by transmission electron microscopy, scale bar is 100 nm. Adapted from ref. 34 (d) this paper tests for local organization in hard, otherwise non-interacting, lattice dimers. Lattice discretization means that our model has unphysically small sea entropy. This unphysical restriction is chosen so we can draw a strong bound on the phenomenon of entropy-driven local organization. *i.e.*, a drawing a strong bound requires pushing deep into the “gray area”, both literally and figuratively.

contexts (see Fig. 1). We model colloidal platelets, imposing a severe restriction on their entropy in which we eliminate their continuum of microstates by discretizing on a lattice. Using the lattice discretization we compute entropic motif preferences (see Fig. 2) by enumerating microstates *via* tensor networks. We find that, albeit weakly, entropy promotes local organization in our lattice model (see Fig. 3 and 4), even in the absence of a continuum sea of microstates. By showing that entropy drives local organization, even in models that have their entropy artificially reduced below what would be expected in any realistic model system, our results suggest that entropy promotes the local organization of crowded, rigid bodies in soft matter and biological systems in general. Finally, by comparing these findings with known results in the literature we establish a

general “road map” (see Fig. 5) for systems to exhibit entropy-driven local organization.

2 Model selection and setup

Determining if entropy generically promotes local organization in soft systems requires a model that can provide a strong bound on the phenomenon. To determine the type of model that will provide such a bound, we briefly recall the circumstances under which entropy is already known to promote local organization.

The phenomenon of entropy-driven local organization is quantitatively well-understood in the context of DEFs, the tendency of colloidal particles to adopt locally dense-packed arrangements.⁶ DEFs were originally hypothesized in three-dimensional crystals of hard, convex, anisotropic colloids with face-to-face, tetrahedral local order.³⁷ Since then, DEFs have been identified in a broad range of other systems,⁶ including crystals of other symmetry in three dimensions,^{6,11,12} plastic crystals,^{13,14} two-dimensional systems and systems with competing enthalpic interactions,¹⁵ non-convex particles,¹⁶ non-polyhedral “entropically patchy” particles,^{6,11} and systems with multiple species of particles,⁶ including depletion interactions.^{3,38} Associated ordering *via* entropy⁷ has been observed in many model^{29–32,39–45} and experimental^{4,5,36,46–50} systems. Apart from colloids, similar entropic effects driving the local organization of crowded objects have been hypothesized⁵¹ or reported in biophysical settings, *e.g.*, in the context of virus–cell–membrane interactions,⁸ or mechano-sensitive membrane channel gating.²⁰

To quantitatively classify systems known to exhibit entropic ordering, we need to first distinguish two different classes of particle interaction: intrinsic and emergent. Intrinsic interactions, such as electrostatic interactions, exist between two particles regardless of the presence of other particles, and can typically be described by a term in the system’s microscopic Hamiltonian. In contrast to intrinsic interactions, emergent interactions do not

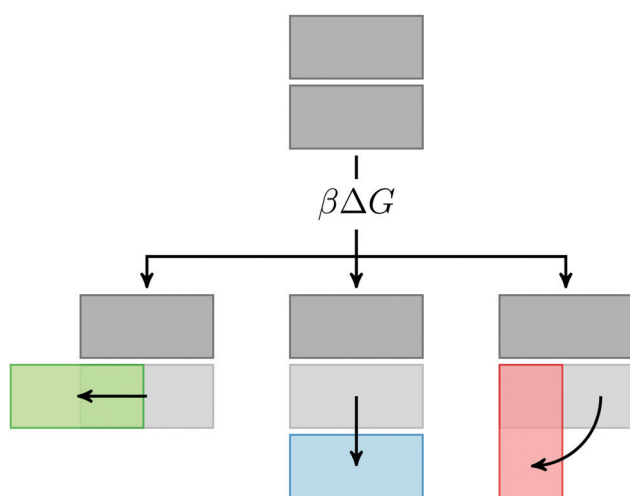


Fig. 2 Entropy-driven local organization is signalled by locally dense-packed dimer configurations (dark grey) having lower free energy ($\beta\Delta G > 0$) compared to configurations in which one of the dimers is displaced horizontally (green) or vertically (blue), or rotated (red) into a less densely-packed motif.

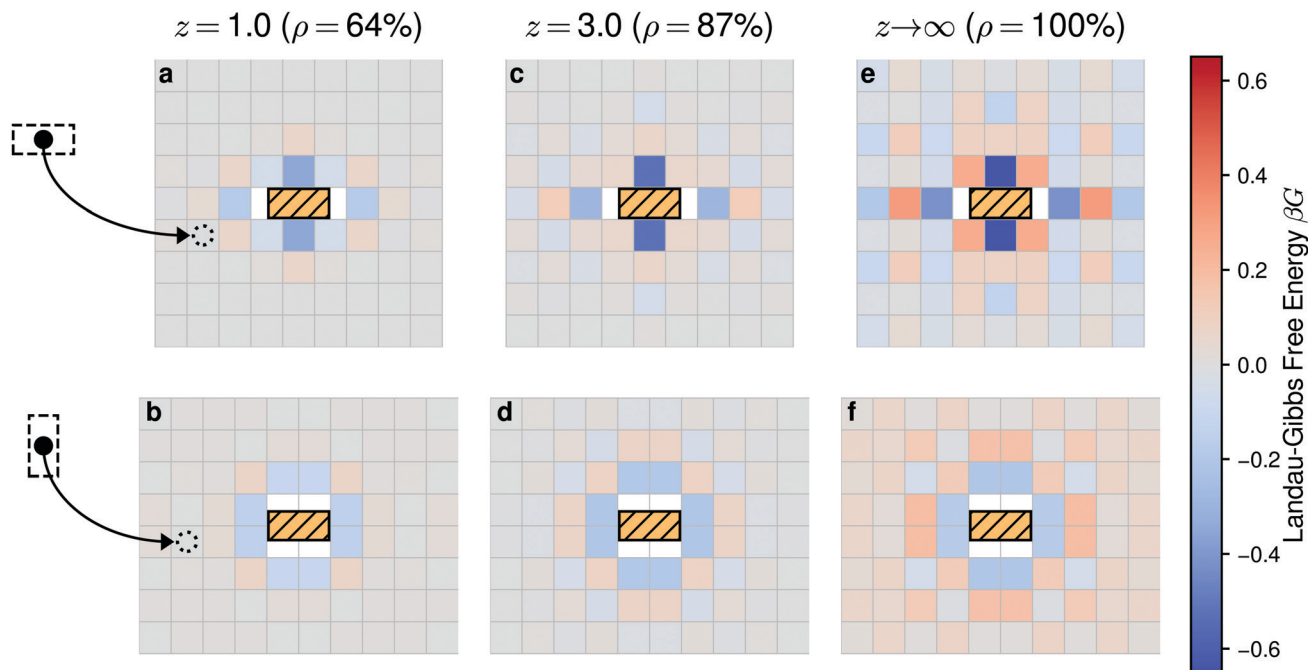


Fig. 3 Landau–Gibbs free energy landscapes show entropy promotes crowded dimers to locally organize. Panels show free energy landscapes for dimer insertion where horizontal and vertical axes correspond to lattice displacement, and colour corresponds to free energy βG . Top row panels (a, c and e) show βG associated with inserting a horizontal dimer (site centres correspond to the location of the inserted horizontal dimer). Bottom row panels (b, d and f) show the βG associated with inserting a vertical dimer (site centres correspond to the location of the inserted vertical dimer). Example insertions are illustrated adjacent to panels (a) and (b). Columns correspond to increasing system fugacity z : $z = 1.0$ for (a and b), $z = 3.0$ for (c and d), $z \rightarrow +\infty$ for (e and f). The deeper blue colours seen for lattice sites adjacent to the central, reference dimer in panels (a, c and e) signal the onset of entropy-driven local organization with increasing density. *I.e.*, compared to other lattice sites in each respective panel, and compared to the fugacity matched panels for vertical insertion (a with b, c with d, e with f), locally dense-packed configurations exhibit the lowest βG . White regions in the plot centres correspond to sterically excluded regions adjacent to the reference dimer. Corresponding densities ρ are indicated, as computed *via* eqn (2).

appear in the microscopic Hamiltonian. Instead, emergent interactions between a selected pair of particles exist due to the mediation of other, “sea” particles.⁶ Determining how sea particles drive the interaction of a selected pair can be done in statistical mechanics by integrating out the sea particles’ degrees of freedom. This integral leaves behind an emergent, effective interaction potential between the remaining particle pair of interest. In liquid state theory the effective interaction potential is known as the potential of mean force;⁵² for anisotropic bodies, it is the potential of mean force and torque (PMFT).⁶ Comparing between prior PMFT computations, *e.g.* ref. 6 and 17, stronger DEFs, and therefore stronger entropic local ordering, exists when the sea particles’ entropy is larger.

The quantitatively clear cases of experimental systems exhibiting entropy-driven local organization fall into three classes: colloid-depletant mixtures,^{5,35} crowded suspensions of three-dimensional colloidal objects,³⁶ and crowded, two-dimensional arrangements of platelets.³⁴ Although all three classes of systems exhibit DEFs, the interaction strength can range from $\sim k_B T$ to $\geq 100 k_B T$ (where k_B is Boltzmann’s constant and T is the temperature). Interactions are strongest in colloid-depletant mixtures. Though they are weaker in monodisperse colloids in three dimensions, and weaker still in two dimensions, effects are still measurable, and sufficient to produce a range of interesting ordered behaviours.^{30,31,53,54}

We aggregate the results from two- and three-dimensional model systems, with and without depletants, and arrange them in order of decreasing sea entropy in Fig. 1a–c, where images are selected to indicate experiments that each represent a class of similar experimental demonstrations. These results suggest that systems with “lots of” entropy, regardless of the specific system details, will manifest entropy-driven local organization in the form of DEFs. To extinguish DEFs, in contrast, the results suggest one should attempt to move rightward in Fig. 1 and “remove the entropy” that could be liberated by forming locally-organized particle arrangements.

To establish a strong lower bound on where entropy can drive local organization, here, we take the entropy removal approach to its extreme and employ a model that we would expect to have less configurational entropy than would exist in any realistic model of a soft or biological system. If we find DEFs persist in a model that has an unrealistically restricted number of particle arrangements, that will imply that any realistic model (anywhere along the axis of Fig. 1), which will necessarily exhibit more entropy, would be a case in which entropy would promote local order.

Following this strategy, provided models remain well-defined, unrealistic entropy restrictions are “features” rather than “bugs” of appropriate model selection for this study. Here, we model colloidal platelets using a lattice discretization, taking the well-known lattice dimer model as a case study.⁵⁵ Each dimer occupies

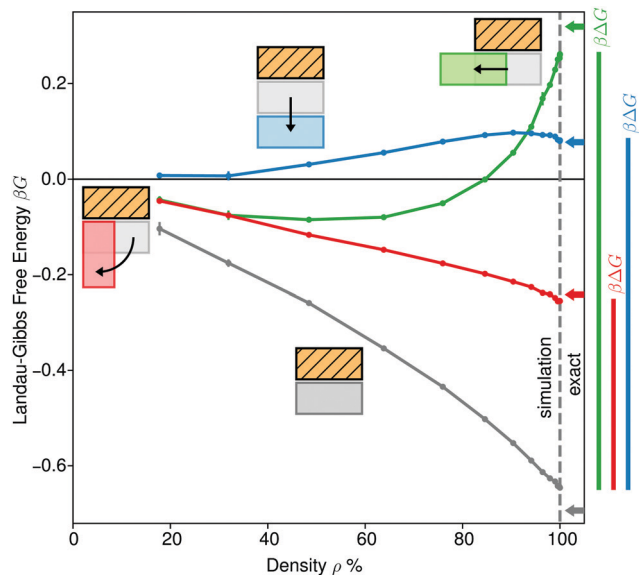


Fig. 4 Landau–Gibbs free energy of lattice dimer motifs shows an increasing preference for local organization with increasing system density. The Landau–Gibbs free energies βG associated with the four configurations described above for a range of densities ρ . Round markers represent the values computed with the tensor network method. Vertical and horizontal error bars are from 3 replica computations, out of them only a few vertical error bars are larger than marker size. Continuous curves are a linear interpolation to guide the eye. The horizontal arrows at $\rho = 100\%$ are the exact values computed in ref. 63. At any fixed density ρ the cost of move between two states $\beta\Delta G$ is given by the difference between the two respective curves. The coloured vertical bars on the right represent the free energy cost of the moves from the paired up configuration (gray) to either of the other three (green, red, blue) at $\rho = 100\%$.

two adjacent lattice sites; the dimers are prohibited from overlapping and that constitutes their only interaction. The lattice dimer model was originally proposed in the 1930s to model adsorption of diatomic molecules on flat surfaces,⁵⁵ but has subsequently been employed in the resonating valence bond model of superconductivity,⁵⁶ and brane tilings in string theory.⁵⁷

One potential pitfall of using a lattice discretization is that whereas a general theorem⁵⁸ precludes the existence of long-range translational order in continuous two-dimensional systems, discrete systems can and do (e.g., the Ising model) manifest long-range order. Fortunately, for the purposes of model selection

for the present study, by leveraging the exact solution at complete tiling,^{59–61} it has been shown that⁶² the model does not exhibit long-range order. This fact indicates that the dimer model is unphysical in a way facilitates drawing a strong entropy bound (removing system entropy), but is not unphysical in a way that would compromise the integrity of its choice in another important respect (manifesting undesirable long-range order). For a brief overview of other results on the dimer model, see the ESI.†

We consider the lattice dimer system on a rectangular domain in the grand canonical ensemble (see Fig. 1d). The ensemble is described by the grand partition function:

$$\mathcal{Z} = \sum_{N,\sigma} z^N, \quad (1)$$

where fugacity $z \equiv e^{\beta\mu} \in [0, \infty)$ is the only free parameter in the model. The fugacity is computed from inverse temperature β and chemical potential μ ; N is the number of sites occupied by dimers (double the number of inserted dimers); and the sum runs over all configurations σ in which no dimers overlap. To determine the existence of entropy-driven local organization, we compute the Landau–Gibbs (LG) free energy difference ($\beta\Delta G$) for dimers in motifs that are locally dense-packed versus those that are not locally dense-packed (see Fig. 2). This LG free energy computation in our lattice model discretizes the PMFT computations done for continuous systems.⁶ As in continuous systems, the development of lower LG free energy in locally dense-packed configurations with increasing system density (fugacity) signals the existence of entropy-driven local organization.

We compute $\beta\Delta G$ using translation symmetry to fix the position of one dimer at the centre of the lattice and enumerating dimer configurations in which a dimer is inserted into one of the adjacent positions, as illustrated in Fig. 2. In the computation, the fixed dimer and the adjacent one form the motif of interest, and all other dimers are treated as sea particles that we integrate out. To perform this integration, we enumerate dimer configurations numerically *via* tensor networks. Details of this computation are described in Methods below.

3 Results

We study local organization by computing the Landau–Gibbs free energy for motifs shown in Fig. 2. We study systems on

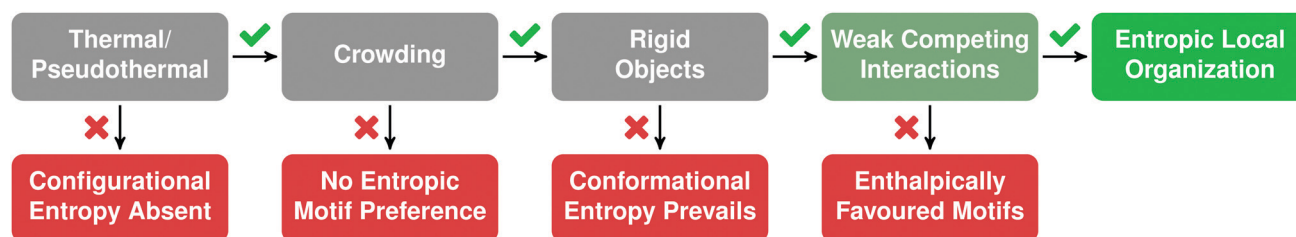


Fig. 5 When does entropy promote local organization? For entropy to promote local organization, systems must be thermal (e.g., ref. 6) or pseudothermal (e.g., ref. 18) to have a meaningful notion of entropy; the constituent objects must be sufficiently crowded (e.g., ref. 6) for entropy to favour local organization; and the objects must be sufficiently rigid so that the free energy cost associated with objects' configurational entropy is low compared to the cost associated with their conformational entropy (e.g., ref. 4). Under those circumstances, entropy will promote local order, but it may not be manifest in experiment unless entropic effects are strong compared to competing interactions (e.g., ref. 34).

rectangular domains of 9×10 sites with periodic boundary conditions. Since the domain has 90 sites and each site can be in 5 different states, this computation requires enumerating $5^{90} \approx 10^{63}$ configurations and counting the ones where none of the dimers overlap. The computation is controlled by fugacity z , however it is more convenient to express results in terms of density ρ , defined as

$$\rho(z) \equiv 1 - p_e^0(z), \quad (2)$$

where $p_e^0(z)$ is the probability that a site of the domain is empty in the absence of the reference dimer (unconstrained network). At zero fugacity $\rho(z=0) = 0\%$ and similarly at infinite fugacity $\rho(z \rightarrow \infty) = 100\%$. After obtaining the density, we constrain the central dimer in the horizontal orientation and compute the free energy landscape for the whole domain. To do so, instead of computing the full partition function, we compute a partial sum, leaving out the degrees of freedom associated with dimers arranged in motifs that correspond to the configurations of interest shown in Fig. 2.

Fig. 3 shows that dense dimers develop entropically preferred motifs with increasing density. The free energy landscapes for the insertion of, separately, horizontal and vertical dimers are presented in Fig. 3 for a series of increasing densities. For horizontal dimers, the landscape retains two two-fold symmetries. For vertical dimers, the landscape develops a four-fold symmetry since all the placements of two adjacent dimers with orthogonal orientations are the same up to a reflection and rotation of the whole system. As we increase the system density, the landscape features sharpen, evident in the emergence of more saturated blue and red colours from the grey background (*e.g.*, compare Fig. 3 panel a with c, and c with e). At the highest density of 100% the free energy maxima and minima reach a finite value, indicating that the DEFs never become infinitely strong. This is expected because it is known that dimers do not have long range order.^{59–61} The local order we do observe, along with the visible oscillating decay of free energy with distance, are consistent with expectations from prior work at perfect tiling.⁶³

The free energy pattern shows a global free energy minimum for pairing the reference horizontal dimer with an immediately adjacent horizontal dimer. This horizontal pairing is a preferred local structure because moving the second dimer left or right, or away from the reference dimer, or rotating it orthogonally all cost free energy.

Having identified both the lowest free energy motif and the immediately adjacent competing motifs, we can further quantify how the strength of DEFs emerges with growing dimer density. We consider three possible symmetry-distinct dimer moves away from the global free energy minimum, as illustrated with different colours in Fig. 2: a horizontal shift, a rotation, and a vertical shift. The density-dependent free energies of dimer placement in each configuration are shown in Fig. 4. The free-energy cost of a move corresponds to the difference between the curves. Note that we avoided computing the curve at low density, since for a domain of 90 sites, inserting a dimer that occupies 2 sites is equivalent to a step in density of almost 2%, thus limiting our density resolution.

Among our results, the largest observed free energy difference $\beta\Delta G$ is around 0.91 for the horizontal shift at density 100% (green bar in Fig. 4). Does this value of $\beta\Delta G$ signify strong DEFs? Note that unlike common Landau free energy computations,⁶⁴ here $\beta\Delta G$ is not scaled by system size and represents the cost of moving a single dimer. One way to interpret this cost is by considering the assembly of a dense-packed dimer crystal in presence of noise. Because of this noise, the ratio of “correctly” placed dimers (dense-packed) to “incorrectly” placed ones (with horizontal shift) is roughly $e^{\beta\Delta G} \sim 2.5 : 1$. For every two correctly placed dimers there would be roughly one defect, thus preventing crystallization and formation of any long-range order, consistent with previous results.⁶²

DEFs in lattice dimers clearly exist, but can they be directly compared with DEFs in other systems? The most obvious comparison system is rectangular platelets of 2:1 aspect ratio with continuous rotations and translations. Such platelets have been considered as a special case in ref. 16 and yielded (canonical) DEF strength of $\beta F \approx 2$. The fact that we observe weaker DEFs in our model system of lattice dimers is consistent with the expectation that putting rectangular platelets on a lattice would reduce the entropy and weaken DEFs. However, we find that although the lattice unreasonably restricts system entropy below what we would expect in a real physical system, system entropy still promotes local order.

4 Discussion

The longstanding,²¹ intuitive association of entropy and disorder suggests that entropy should, in general, act to inhibit organization in soft matter and biological systems. However, the intuition that entropy inhibits organization has been shown to fail in several remarkable counter examples.^{6,7} The need to understand the pattern underlying those counter examples raises the question posed by our title: when does entropy promote local organization?

Based on the observation of weaker patterns of local organization with decreasing amounts of sea entropy, here we sought to establish a bound by extremizing sea entropy. Fig. 4 shows that even with unphysically stringent restrictions imposed by the model we considered here, *i.e.*, that it lacks a continuum of sea entropy, entropy still promoted, rather than inhibited, local organization.

Collectively, the results in the literature and the results presented here show that entropy promotes local order over the entire range shown in Fig. 1. This range spans physically reasonable amounts of sea entropy and extends beyond. This range is surprising because although early, and striking, examples of entropic local organization involved depletion interactions,³ where sea entropy is particularly large, depletion is not necessary for local organization. Our results further show that any physically reasonable amount (and even less!) of sea entropy is enough configurational entropy to promote local organization. That means an answer to the question of when entropy promotes local organization does not involve sea entropy.

If the amount of sea entropy is not a limiting factor for the entropic promotion of local organization, what is? Experiments

indicate both synthetic (*e.g.*, ref. 47) and biological (*e.g.*, ref. 9) systems exhibit the entropic promotion of local organization. However, work on colloids⁶ indicates that some form of crowding of objects is required, either from the existence of depletion interactions³ or *via* “self-depletion” of the constituent objects.⁶ In addition to crowding, limitations on entropic local organization could arise from a lack of thermalization, from system scale, or from system rigidity. Whether these considerations impose limitations on entropy-driven local organization can be inferred from the existing experimental literature.

Thermalization

Colloidal systems with clearly quantifiable entropic local organization, *e.g.*, ref. 6, manifest those effects in systems in thermal equilibrium. Since entropy is most clearly defined in thermal equilibrium, that appears to suggest that entropy-driven local order depends fundamentally on the existence of thermodynamic equilibrium. However, the hallmarks of entropy-driven local organization have been demonstrated in experiments performed on pseudo-thermally-driven granular systems.¹⁸ Those experiments indicate that a pseudothermal approximation of configurational entropy is to manifest entropically-driven local organization.

Scale

Many physical phenomena are system scale dependent, and so scale could constrain the entropic promotion of local organization. Colloidal systems manifest the most clearly identifiable instances of entropic local organization for particles in the range of hundreds of nanometres, *e.g.*, ref. 47. However, similar effects exist for particles toward the nanometre range, *e.g.*, ref. 34, and for granular systems with particles that are millimetres in size.¹⁸ The roughly five orders of magnitude in particle scale between these systems strongly suggests that scale does not restrict entropy-driven local organization.

Rigidity

Entropic local organization has been demonstrated in systems of rigid objects, *e.g.*, in hard colloids.⁶ However, work by Dogic and collaborators suggests that the rigidity of constituent objects is a limiting factor.^{4,65,66} Dogic *et al.* demonstrated the entropy-driven assembly, *via* depletion, of rod-shaped virus capsids into non-amphiphilic membranes. The assembled membranes in Dogic's experiments were themselves objects that could undergo hierarchical entropy-driven assembly into rouleaux, columnar structures also observed in red blood cell aggregates.³ However, hierarchical rouleaux assembly was only observed if the depletion interactions driving the assembly resulted in high membrane tension. At low membrane tension, the large conformational entropy of the membranes inhibited their organization into rouleaux. In the context of the present discussion, Dogic *et al.*'s results suggest that entropy inhibits local organization if the objects undergoing the local organization would lose internal, conformational entropy through steric restriction imposed by local organization. This interpretation also accords with a recent study¹⁰ on the effects of the rigidity and shape of hydrocarbon molecules in self-assembly. There, it

was shown that conformational entropy in linear alkanes inhibits molecular self-assembly compared with rigid diamondoid molecules. Together, the virus-capsid and alkane results, taken in contrast with the results here and elsewhere for rigid colloids, indicate that in crowded systems there is a competition between the entropic promotion of local organization by configurational entropy and the inhibition of local organization by conformational entropy.

The considerations of thermalization, scale, and rigidity lead us to propose Fig. 5 as an answer to the question of when does entropy promote local organization? In addition to the criteria regarding configurational entropy, crowding, and rigidity that are included in Fig. 5, it is also noteworthy that seemingly relevant criteria, *e.g.*, depletion interactions or system scale, turn out to be “non-factors” for the entropic promotion of local organization.

Although, Fig. 5 serves as a guide for the circumstances under which entropy should be expected to promote local organization, there is also the question of when entropically favoured motifs will manifest in experiment. For entropic motifs to be manifest, the strength of the entropically preferred motifs must be sufficiently strong compared to non-entropic interactions. We indicate this accordingly in Fig. 5. Ref. 34 reports an example of this, and ref. 17 reports an approach to estimate the strength of competing interactions required to overwhelm entropic forces.

The minimal restrictions on entropic local organization arising only from configurational entropy, crowding, rigidity, and competing interactions (Fig. 5), and the manifestation of these effects across scales ranging from nanometres to millimetres suggest the potential for exploiting the entropic organization in a broad range of molecular, soft matter, granular, and biological contexts.^{4,5,8,9,18,20,36,46,47,67}

5 Methods

5.1 Partition function setup

We treated the lattice dimer model numerically as a spin-like model on a square lattice. Each lattice site *i* can be in one of five states *s_i*, either the site is empty *e*, or it is occupied by the left *l*, right *r*, top *t*, or bottom *b* part of a dimer. The latter four states correspond to site occupation with half a dimer so that fixing a spin state on any site constrains the spin on neighbouring sites. Horizontally, for example, a site to the right of an *l* state (*i.e.*, a left half-dimer) must be occupied by an *r* state (*i.e.*, a right half-dimer) and cannot be occupied by an *l*, *t*, *b*, or *e* state. Similar constraints exist for vertical neighbours. We penalize violating the set of these neighbour constraints with an infinite energy penalty in a local Hamiltonian *H*, which is otherwise zero. We treat the dimer model in the grand canonical ensemble with partition function \mathcal{Z} given by

$$\mathcal{Z} = \sum_{\{s\}} e^{-\beta H(\{s\})} \prod_i f(s_i), \quad (3)$$

where β is the inverse temperature, and $f(s_i) = 1$ for empty sites ($s_i = e$) and $e^{\beta\mu}$ (with μ being the chemical potential) otherwise. In this form, the problem of describing the physics of lattice

dimer configurations reduces to enumerating arrangements of “spins” that satisfy the appropriate constraints.

To enumerate arrangements of spins, we extend recently-proposed^{68,69} methods that attack solution counting problems with tensor networks. Tensor networks derived from an early graphical notation⁷⁰ are now used in quantum condensed matter systems,^{71–73} quantum chemistry,⁷⁴ the renormalization of classical lattice models,^{75,76} machine learning,⁷⁷ and numerical linear algebra.^{78–80} To apply tensor network methods here, we first note that because the model Hamiltonian H has only zero or infinite entries, the corresponding Boltzmann factors $e^{-\beta H}$ are 1 or zero, respectively. The Boltzmann factors for horizontally and vertically adjacent spins can be combined into horizontal ($T_{s_i s_j}^h$) and vertical ($T_{s_i s_j}^v$) transfer matrices⁶⁴ that encode the constraints against “breaking” dimers (explicit forms are given in ESI†). In terms of T^h and T^v the partition function takes the form

$$\mathcal{Z} = \sum_{\{s\}} \prod_{\langle ij \rangle_h} T_{s_i s_j}^h \prod_{\langle ij \rangle_v} T_{s_i s_j}^v \prod_i f(s_i), \quad (4)$$

where $\langle \rangle_{h,v}$ denotes horizontal and vertical nearest neighbour pairs. In this form, \mathcal{Z} is contraction of a tensor network with transfer matrices $T^{h,v}$ taken as rank-2 tensors and f as a rank-1 tensor. Apart from those three types of tensors, we include a fourth type: site tensors δ . Each site tensor is a multidimensional Kronecker (identity) tensor that connects to all the neighbours in an appropriate order (see Fig. 6). The site tensors only contribute multiplicative factors of 1 to the sum (4) and thus do not change the result. The raw value of the partition function at $\rho = 100\%$ density is directly related to a measure of dimer configurations, the so-called “molecular freedom”, for which an exact analytic value is known.^{59–61} We use the known molecular freedom to validate our computational method (see ESI†).

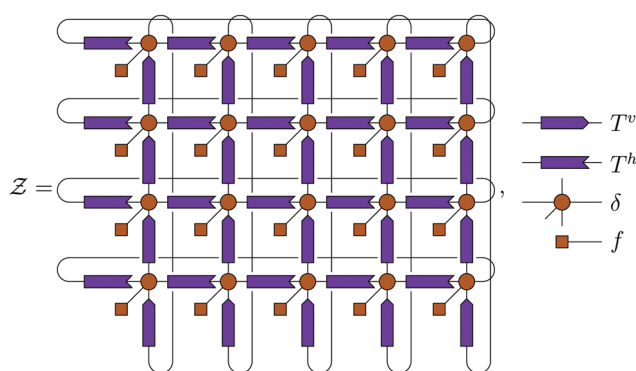


Fig. 6 Lattice spin partition functions can be expressed in terms of tensor networks. Here, for illustration purposes, we show a 4×5 lattice where lattice sites correspond to identity tensors ($\delta_{s_i s_j \dots}$, brown circles). Coupling tensors, generalizations of transfer matrices, couple spins on vertically ($T_{s_i s_j}^v$, purple arrows) or horizontally ($T_{s_i s_j}^h$, purple tails) neighbouring sites. Both types of coupling tensors are asymmetric in their indices, therefore the direction of arrows and tails is important. The fugacity tensor (f_{s_i} , brown square), promotes the insertion of dimers. “Legs” on tensor symbols correspond to spin indices and connected legs correspond to summation, or contraction, of the network, as in eqn (4).

5.2 Landau–Gibbs free energy evaluation

Eqn (4) gives a recipe for computing the partition function, but we aim to study local organization by comparing dimer motifs by their respective Landau–Gibbs free energies. Lower LG free energy in locally dense-packed configurations with increasing system density (fugacity) signifies the existence of entropically favoured motifs. Disfavoured motifs are signified by higher free energy. The LG free energy quantifies the probability of finding a dimer in a specific motif, as opposed to finding a dimer by itself (bare):

$$\beta G = \beta G_{\text{motif}} - \beta G_{\text{bare}}, \quad (5)$$

where G_{bare} is the free energy of finding a dimer in a given orientation by itself, which depends on the fugacity $z = e^{\beta \mu}$ but not on the dimer position. G_{motif} is the free energy of finding a dimer in a given motif with respect to a fixed reference dimer, which thus depends on both the fugacity and the relative position of the dimers. The two free energies are computed as following:

$$e^{-\beta G_{\text{bare}}(s)} \propto \sum_{\{s\} - \{s_{x,y}\}} \prod_{\langle ij \rangle_h} T_{s_i s_j}^h \prod_{\langle ij \rangle_v} T_{s_i s_j}^v \prod_i f(s_i), \quad (6)$$

$$e^{-\beta G_{\text{motif}}(s;x,y)} \propto \sum_{\{s\} - \{s_{x,y}\}} \prod_{\langle ij \rangle_h} T_{s_i s_j}^h \prod_{\langle ij \rangle_v} T_{s_i s_j}^v \prod_i f(s_i) \delta(\text{ref}), \quad (7)$$

where x, y is the site for which we are computing the free energy and thus we exclude its spin variable $s_{x,y}$ from summation. We fix the reference dimer in a specific state with the constraint $\delta(\text{ref})$. Each free energy is normalized so that the exponential factors for all $s_{x,y}$ add up to 1. The expressions (6) and (7) can be both shown succinctly using the graphic notation and evaluated numerically as tensor network contractions (see ESI†).

We perform the numerical tensor network contractions with PyTNR, an open-source, general purpose tensor-network contraction code.^{81,82} PyTNR contracts networks using singular value decomposition (SVD), as a numerical approximation. This approximation allows the counting of huge numbers of states to remain tractable at the expense of applying SVD to intermediate tensors in the contraction procedure in stochastic order. To control for the statistical errors resulting from stochasticity we computed at least three replicas at each statepoint. To control for the systematic error of finite system size we performed finite-size validation against the known correlation functions at $\rho = 100\%$ density (see ESI†). The largest networks we contracted correspond to $15 \times 16 = 240$ lattice sites, and thus enumerate $5^{240} \approx \mathcal{O}(10^{167})$ distinct lattice spin states.

To reconstruct the full LG free energy landscapes in Fig. 3, we compute a large number of motif free energies $G_{\text{motif}}(s_m)$ for different target sites m . We reduce the number of required computations with two strategies. First, we take advantage of the global four-fold mirror symmetry of the system and the local translational symmetry of the sites (see ESI†). Second, we create an additional readout tensor network that implements efficient multi-marginalizing, *i.e.* computation of 1-point marginals from a many-point distribution (see ESI†).‡

‡ We learned about multi-marginalizing from A. S. Jermyn who also implemented it as a part of the PyTNR package.

Conflicts of interest

There are no conflicts to declare.

Acknowledgements

GvA acknowledges the support of the Natural Sciences and Engineering Research Council of Canada (NSERC). We thank A. S. Jermyn for technical support of the PyTNR package, as well as S. Boettcher, M. P. Brenner, C. R. Doering, C. X. Du, and H. Liu, for stimulating discussions.

Notes and references

- J. N. Israelachvili, *Intermolecular and Surface Forces*, Academic Press, Burlington, MA, 3rd edn, 2011.
- V. N. Manoharan, *Science*, 2015, **349**, 942.
- H. N. W. Lekkerkerker and R. Tuinier, *Colloids and the Depletion Interaction*, Springer, Dordrecht, 2011.
- E. Barry and Z. Dogic, *Proc. Natl. Acad. Sci. U. S. A.*, 2010, **107**, 10348–10353.
- K. L. Young, M. R. Jones, J. Zhang, R. J. Macfarlane, R. Esquivel-Sirvent, R. J. Nap, J. Wu, G. C. Schatz, B. Lee and C. A. Mirkin, *Proc. Natl. Acad. Sci. U. S. A.*, 2012, **109**, 2240–2245.
- G. van Anders, D. Klotsa, N. K. Ahmed, M. Engel and S. C. Glotzer, *Proc. Natl. Acad. Sci. U. S. A.*, 2014, **111**, E4812–E4821.
- D. Frenkel, *Nat. Mater.*, 2015, **14**, 9–12.
- J. J. Madsen, J. M. Grime, J. S. Rossman and G. A. Voth, *Proc. Natl. Acad. Sci. U. S. A.*, 2018, **115**, E8595–E8603.
- C. Wagner, P. Steffen and S. Svetina, *C. R. Phys.*, 2013, **14**, 459–469.
- E. M. King, M. A. Gebbie and N. A. Melosh, *Langmuir*, 2019, **35**, 16062–16069.
- G. van Anders, N. K. Ahmed, R. Smith, M. Engel and S. C. Glotzer, *ACS Nano*, 2014, **8**, 931–940.
- Y. Geng, G. van Anders, P. M. Dodd, J. Dshemuchadse and S. C. Glotzer, *Sci. Adv.*, 2019, **5**, eaaw0514.
- W. Shen, J. Antonaglia, J. A. Anderson, M. Engel, G. van Anders and S. C. Glotzer, *Soft Matter*, 2019, **15**, 2571–2579.
- A. S. Karas, J. Dshemuchadse, G. van Anders and S. C. Glotzer, *Soft Matter*, 2019, **15**, 5380–5389.
- J. A. Millan, D. Ortiz, G. van Anders and S. C. Glotzer, *ACS Nano*, 2014, **8**, 2918–2928.
- E. S. Harper, R. L. Marson, J. A. Anderson, G. van Anders and S. C. Glotzer, *Soft Matter*, 2015, **11**, 7250–7256.
- E. S. Harper, G. van Anders and S. C. Glotzer, *Proc. Natl. Acad. Sci. U. S. A.*, 2019, **116**, 16703–16710.
- L. Walsh and N. Menon, *J. Stat. Mech.: Theory Exp.*, 2016, 083302.
- H. Bäuml, B. Neu, E. Donath and H. Kieseewetter, *Biorheology*, 1999, **36**, 439–442.
- M. Lindén, P. Sens and R. Phillips, *PLoS Comput. Biol.*, 2012, **8**, e1002431.
- R. Clausius, *Abhandlungen Über Die Mechanische Wärmetheorie*, Friedrich Vieweg und Sohn, Braunschweig, 1864.
- The Many-Body Problem*, ed. J. K. Percus, Interscience Publishers, New York, 1963.
- L. Onsager, *Ann. N. Y. Acad. Sci.*, 1949, **51**, 627–659.
- B. J. Alder and T. E. Wainwright, *J. Chem. Phys.*, 1957, **27**, 1208–1209.
- W. W. Wood and J. D. Jacobson, *J. Chem. Phys.*, 1957, **27**, 1207–1208.
- P. N. Pusey and W. van Megen, *Nature*, 1986, **320**, 340–342.
- D. Frenkel, *J. Phys. Chem.*, 1987, **91**, 4912–4916.
- D. Frenkel, *Phys. A*, 1999, **263**, 26–38.
- A. Haji-Akbari, M. Engel, A. S. Keys, X. Zheng, R. G. Petschek, P. Palfy-Muhoray and S. C. Glotzer, *Nature*, 2009, **462**, 773–777.
- U. Agarwal and F. A. Escobedo, *Nat. Mater.*, 2011, **10**, 230–235.
- P. F. Damasceno, M. Engel and S. C. Glotzer, *Science*, 2012, **337**, 453–457.
- J. de Graaf, R. van Roij and M. Dijkstra, *Phys. Rev. Lett.*, 2011, **107**, 155501.
- R. Cersonsky, G. van Anders, P. M. Dodd and S. C. Glotzer, *Proc. Natl. Acad. Sci. U. S. A.*, 2018, **115**, 1439–1444.
- X. Ye, C. Jun, M. Engel, J. A. Millan, W. Li, L. Qi, G. Xing, J. E. Collins, C. R. Kagan, J. Li, S. C. Glotzer and C. B. Murray, *Nat. Chem.*, 2013, **5**, 466–473.
- S. Sacanna, W. T. M. Irvine, P. M. Chaikin and D. Pine, *Nature*, 2010, **464**, 575–578.
- J. Henzie, M. Grünwald, A. Widmer-Cooper, P. L. Geissler and P. Yang, *Nat. Mater.*, 2012, **11**, 131–137.
- P. F. Damasceno, M. Engel and S. C. Glotzer, *ACS Nano*, 2012, **6**, 609–614.
- D. J. Kraft, R. Ni, F. Smallenburg, M. Hermes, K. Yoon, D. A. Weitz, A. van Blaaderen, J. Groenewold, M. Dijkstra and W. K. Kegel, *Proc. Natl. Acad. Sci. U. S. A.*, 2012, **109**, 10787–10792.
- R. Ni, A. P. Gantapara, J. de Graaf, R. van Roij and M. Dijkstra, *Soft Matter*, 2012, **8**, 8826–8834.
- A. P. Gantapara, J. de Graaf, R. van Roij and M. Dijkstra, *Phys. Rev. Lett.*, 2013, **111**, 015501.
- F. A. Escobedo, *Soft Matter*, 2014, **10**, 8388–8400.
- C. Avendano and F. A. Escobedo, *Soft Matter*, 2012, **8**, 4675–4681.
- F. Smallenburg, L. Filion, M. Marechal and M. Dijkstra, *Proc. Natl. Acad. Sci. U. S. A.*, 2012, **109**, 17886–17890.
- D. Klotsa, E. R. Chen, M. Engel and S. C. Glotzer, *Soft Matter*, 2018, **14**, 8692–8697.
- C. Avendano and F. A. Escobedo, *Curr. Opin. Colloid Interface Sci.*, 2017, **30**, 62–69.
- K. L. Young, M. L. Personick, M. Engel, P. F. Damasceno, S. N. Barnaby, R. Bleher, T. Li, S. C. Glotzer, B. Lee and C. A. Mirkin, *Angew. Chem., Int. Ed.*, 2013, **52**, 13980–13984.
- L. Rossi, S. Sacanna, W. T. M. Irvine, P. M. Chaikin, D. J. Pine and A. P. Philipse, *Soft Matter*, 2011, **7**, 4139–4142.
- A. V. Petukhov, R. Tuinier and G. J. Vroege, *Curr. Opin. Colloid Interface Sci.*, 2017, **30**, 54–61.
- A. Perro, S. Reculosa, S. Ravaine, E. Bourgeat-Lami and E. Duguet, *J. Mater. Chem.*, 2005, **15**, 3745–3760.

- 50 A. Désert, C. Hubert, Z. Fu, L. Moulet, J. Majimel, P. Barboiteau, A. Thill, M. Lansalot, E. Bourgeat-Lami, E. Duguet and S. Ravaine, *Angew. Chem., Int. Ed.*, 2013, **52**, 11068–11072.
- 51 M. S. Cheung and A. G. Gasic, *Phys. Biol.*, 2018, **15**, 063001.
- 52 J.-P. Hansen and I. McDonald, *Theory of Simple Liquids*, Elsevier, 2006.
- 53 J. A. Anderson, J. Antonaglia, J. A. Millan, M. Engel and S. C. Glotzer, *Phys. Rev. X*, 2017, **7**, 021001.
- 54 A. P. Gantapara, W. Qi and M. Dijkstra, *Soft Matter*, 2015, **11**, 8684–8691.
- 55 R. H. Fowler and G. S. Rushbrooke, *Trans. Faraday Soc.*, 1937, **33**, 1272–1294.
- 56 D. S. Rokhsar and S. A. Kivelson, *Phys. Rev. Lett.*, 1988, **61**, 2376–2379.
- 57 K. D. Kennaway, *Int. J. Mod. Phys. A*, 2007, **A22**, 2977–3038.
- 58 N. D. Mermin and H. Wagner, *Phys. Rev. Lett.*, 1966, **17**, 1133.
- 59 P. Kasteleyn, *Physica*, 1961, **27**, 1209–1225.
- 60 H. N. V. Temperley and M. E. Fisher, *Philos. Mag.*, 1961, **6**, 1061–1063.
- 61 M. E. Fisher, *Phys. Rev.*, 1961, **124**, 1664.
- 62 P. W. Kasteleyn, *J. Math. Phys.*, 1963, **4**, 287–293.
- 63 M. E. Fisher and J. Stephenson, *Phys. Rev.*, 1963, **132**, 1411.
- 64 N. Goldenfeld, *Lectures on phase transitions and the renormalization group*, Addison-Wesley, Reading MA, 1992.
- 65 Y. Yang, E. Barry, Z. Dogic and M. F. Hagan, *Soft Matter*, 2012, **8**, 707–714.
- 66 T. Gibaud, E. Barry, M. J. Zakhary, M. Henglin, A. Ward, Y. Yang, C. Berciu, R. Oldenbourg, M. F. Hagan, D. Nicastro, R. B. Meyer and Z. Dogic, *Nature*, 2012, **481**, 348–351.
- 67 K. Drescher, J. Dunkel, C. D. Nadell, S. Van Teeffelen, I. Grnja, N. S. Wingreen, H. A. Stone and B. L. Bassler, *Proc. Natl. Acad. Sci. U. S. A.*, 2016, **113**, E2066–E2072.
- 68 J. D. Biamonte, J. Morton and J. Turner, *J. Stat. Phys.*, 2015, **160**, 1389–1404.
- 69 S. Kourtis, C. Chamon, E. R. Mucciolo and A. E. Ruckenstein, *SciPost Phys.*, 2019, **7**, 060.
- 70 R. Penrose, *Combinatorial Mathematics and its Applications*, 1971, vol. 1, pp. 221–244.
- 71 F. Verstraete, V. Murg and J. I. Cirac, *Adv. Phys.*, 2008, **57**, 143–224.
- 72 U. Schollwöck, *Ann. Phys.*, 2011, **326**, 96–192.
- 73 R. Orús, *Ann. Phys.*, 2014, **349**, 117–158.
- 74 G. K.-L. Chan and S. Sharma, *Annu. Rev. Phys. Chem.*, 2011, **62**, 465–481.
- 75 Z. Xie, H. Jiang, Q. Chen, Z. Weng and T. Xiang, *Phys. Rev. Lett.*, 2009, **103**, 160601.
- 76 M. Levin and C. P. Nave, *Phys. Rev. Lett.*, 2007, **99**, 120601.
- 77 E. Stoudenmire and D. J. Schwab, *Advances in Neural Information Processing Systems*, 2016, pp. 4799–4807.
- 78 A. Cichocki, N. Lee, I. Oseledets, A.-H. Phan, Q. Zhao and D. P. Mandic, *et al.*, *Foundations and Trends in Mach. Learn.*, 2016, **9**, 249–429.
- 79 A. Cichocki, A.-H. Phan, Q. Zhao, N. Lee, I. Oseledets, M. Sugiyama and D. P. Mandic, *et al.*, *Foundations and Trends in Mach. Learn.*, 2017, **9**, 431–673.
- 80 I. V. Oseledets, *SIAM J. Sci. Comput.*, 2011, **33**, 2295–2317.
- 81 A. S. Jermyn, *SciPost Phys.*, 2020, **8**, 5.
- 82 A. S. Jermyn, *J. Comput. Phys.*, 2019, **377**, 142–154.